Dynamic Harmonic Mitigation via Optimized PI-Controlled SAPF Considering Utility Voltage Distortion and Load Variations

Ahmed Mohammed Attiya Soliman[*,**‡], Mohammed Hamouda Ali[**],
Abdelmoezz Ahmed Eid[**], Sally El-Tawab[**]

[*] Department of Electrical Engineering, College of Engineering, University of Bisha, P.O. Box 551, Bisha 61922, Saudi Arabia.

[**] Department of Electrical Engineering, Faculty of Engineering, Al-Azhar University, P.O. Box 11751, Cairo 11884, Egypt.

(asoliman@ub.edu.sa , Eng_ahmed1020@azhar.edu.eg, Eng_MohammedHamouda@azhar.edu.eg, engabdelmoezz@azhar.edu.eg, sally.eltawab@azhar.edu.eg)

[‡] Corresponding Author; Ahmed Mohammed Attiya Soliman, University of Bisha, P.O. Box 551, Bisha 61922, Saudi Arabia, asoliman@ub.edu.sa.

Received: 23.06.2025 Accepted: 23.11.2025

Abstract-This study addresses the persistent challenge of harmonic distortion in electrical distribution systems (EDSs) caused by nonlinear loads (NLL) and grid voltage irregularities. It proposes an optimized control strategy for a Shunt Active Power Filter (SAPF) to enhance power quality (PQ) and maintain system stability under varying operating conditions. The core methodology integrates a proportional–integral (PI) controller, combined with a hysteresis current control technique (HCCT), to manage both DC-link voltage and synchronization. This is achieved via a Phase-Locked Loop (PLL) coupled with a Positive Sequence Voltage Detector (PSVD), introducing both conventional and adaptive controller techniques. This paper conducts a comparative analysis of a proposed controller technique with and without tuned and optimized PI controller gains in both the PLL and DC-link voltage circuits, evaluating the performance of the SAPF controller. Optimization of controller parameters is achieved through the Dandelion Optimizer (DO), a recent metaheuristic algorithm benchmarked against Aquila Optimizer (AO), Mayfly Optimization Algorithm (MOA), and War Strategy Optimizer (WSO). MATLAB/Simulink simulations test conventional and adaptive SAPF configurations under diverse conditions, including voltage distortion and dynamic load variations. Results show that the DO-optimized controllers significantly outperform non-optimized cases, meeting key objectives and exhibiting superior dynamic response, minimal steady-state error, and a total harmonic distortion (THD) reduced to below the IEEE standard limits. The novelty lies in applying the DO algorithm for the first time to SAPF parameter optimization within smart grid environments, achieving robust, self-adaptive harmonic mitigation and stable power quality improvement across fluctuating grid and load scenarios. The work confirms the DO's superiority in achieving fast convergence and optimal tuning for enhanced electrical performance and reliability, contributing to the development of intelligent, resilient smart power systems.

Keywords Shunt active power filter, proportional integral controller, metaheuristic optimization algorithm, dandelion optimizer, total harmonic distortion, power quality.

1. Introduction

Power quality (PQ) has become a critical concern for utilities and consumers alike, driven by the growing penetration of nonlinear loads (NLLs) and renewable energy sources. These systems employ power electronics-based switching devices. The proliferation of power electronics-based devices has significantly degraded PQ in electrical supply systems [1,2]. They distort voltage and current waveforms, injecting harmonic currents into the distribution

network. These harmonics further propagate into system voltages, disrupting the operation of distribution equipment and causing disturbances that are highly sensitive to deviations from ideal sinusoidal voltage [3,4]. These disturbances spread to consumer equipment connected at the point of common coupling (PCC), deteriorating PQ and leading to several operational issues. They are primarily responsible for reduced system efficiency (evidenced by elevated total harmonic distortion (THD) and poor power factor), increased transmission losses, overheating of electrical devices, premature equipment failure, and malfunctioning of sensitive components. Additionally, they can cause capacitor explosions, protection system misoperations, and electromagnetic interference (EMI) in communication systems [5-9].

Therefore, it is essential to limit harmonic distortion and maintain it within acceptable levels to reduce power quality issues. Consequently, harmonic filters are installed to effectively reduce current distortion and reactive power [10,11]. Several harmonic mitigation strategies are documented in the literature, including passive power filters (PPFs) [12], active power filters (APFs) [13], and hybrid power filters (HPFs) [14,15]. APFs comprise series [16], shunt [17-23], and a unified power quality conditioner (UPQC) [24,25] topologies. Where the latter is a combination of series and shunt APFs in one configuration. Also, HPF combines PPF and APF, such as the Hybrid Series Active Power filter [26] and the Hybrid Shunt Active Power filter [27].

Conventional solutions like PPFs, while historically used for harmonic mitigation, are proving insufficient for contemporary power quality requirements. PPFs present inherent drawbacks such as parallel resonance with grid impedance, excessive reactive power compensation at fundamental frequency, and inadequate dynamic response to varying harmonic spectra [1,14]. The escalating severity of power quality (PQ) issues in modern grids has prompted power engineers to devise adaptive solutions capable of addressing dynamic PQ challenges. Among these, APFs, or active power line conditioners, provide broad compensation capabilities. They mitigate harmonics, correct reactive power, regulate voltage, suppress flicker, and balance three-phase voltages. In addition, APFs offer several key advantages: they automatically adjust to network variations and load changes, mitigate multiple harmonic orders, remain unaffected by significant grid characteristic modifications, eliminate filter-network resonance risks, and require substantially less space than conventional passive compensators [1]. These capabilities make APFs the preferred intelligent solution for harmonic mitigation, as they actively identify distortions and inject corrective currents to enhance power quality [2,3,5,10,13,14,21].

APF technology combines power electronic switching devices with passive energy storage components (capacitors and inductors) and can be categorized based on several key factors: (1) connection method to the power system (series or shunt), (2) power rating (low, medium, or high power), (3) converter type (current-source or voltage-source converters), (4) converter topology (inverter, switch-capacitor, or hybrid), (5) system configuration (two-wire for single-phase or three/four-wire for three-phase systems), (6) control strategies (proportional-integral (PI), instantaneous power, or dq theories), and (7) compensation objectives (current/voltage harmonics, reactive power, power factor correction, three-phase balancing, or combinations of them) [1,7,13].

Recent research has demonstrated that shunt active power filters (SAPFs) represent the most efficient solution for mitigating harmonic current issues in power systems. Therefore, this study focuses on a SAPF that measures the harmonic current distortion present in the power system. Based on this measurement, it generates and injects a compensatory current at the PCC. The generated current, equal in magnitude but shifted by 180°, effectively eliminates harmonic contamination, resulting in a sinusoidal source current that maintains phase alignment with the supply voltage. These results are realized when all control system components function as intended. This fundamental concept remains valid for all harmonic-producing load types. Furthermore, through proper control strategy implementation, the APF can additionally provide power factor correction. Consequently, the power distribution system perceives the combined NLL and APF as a purely resistive element, thereby satisfying all required SAPF compensation objectives [1,7].

SAPFs typically utilize Pulse Width Modulated Voltage Source Inverters (PWM-VSI) configured as current-controlled devices. These systems function as non-sinusoidal current sources connected at the PCC, designed to supply the harmonic current demands of nonlinear loads. While SAPFs demonstrate superior filtering capabilities, their performance relies on both the power circuit design and the implemented control strategy. The control algorithm plays a pivotal role in harmonic mitigation, executing four critical functions: computing reference current waveforms for each inverter phase, maintaining constant DC-link voltage, controlling synchronization, and generating precise gating signals through the current control system. The SAPF control scheme operates through two primary stages, as illustrated in Figure 1. The first stage employs fast-response time-domain controllers to derive compensation signals instantaneously. This reference current extraction process identifies the harmonic components in the load current and generates corresponding compensation currents for injection at the PCC. The second stage implements current control techniques to produce precise gating signals or pulses for the PWM-VSI. By regulating the inverter's switching devices according to the extracted reference signals, this stage ensures optimal compensation performance [1,28].

For the harmonic identification method to calculate the reference currents for SAPF, there are many methods for harmonic identification, such as instantaneous power, synchronous reference frame (SRF), synchronous detection (SD), a a-b-c reference frame, and a dq-axis with Fourier (dqF). For current injection control, common approaches include the hysteresis current control technique (HCCT) and PWM. DC link voltage regulation can be achieved through various controllers, such as PI or fuzzy logic controllers

(FLCs) [1,2,6,7,29]. In this paper, the PI controller is applied to estimate the reference current with and without positive-sequence detectors (PSD). Also, the PI controller is employed to control the DC bus voltage, and the gating signals are obtained based on HCCT.

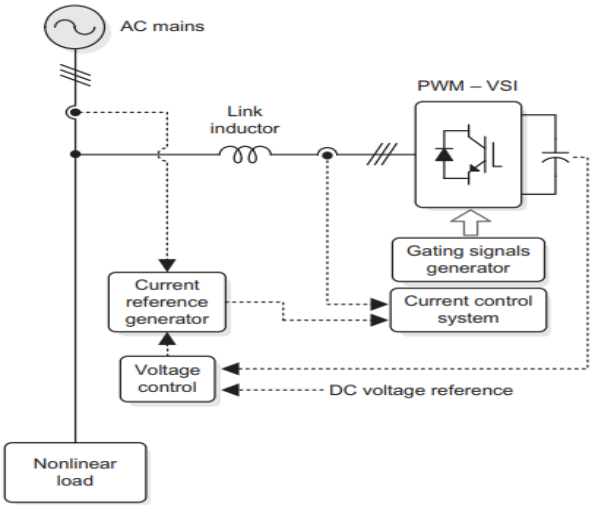

Fig. 1. Control scheme of (SAPF).

Despite the effectiveness of SAPFs, several technical challenges must be resolved for successful SAPF integration into power systems with harmonic pollution. A particularly crucial challenge involves achieving perfect grid synchronization, maintaining simultaneous frequency matching, and phase alignment for stable, continuous harmonic mitigation. As illustrated in Figure 2, an optimal synchronization technique must: accurately track grid voltage phase angles, detect and adapt to frequency fluctuations, filter high-frequency harmonics, and rapidly respond to grid voltage variations [7].

Synchronization techniques in SAPF control systems vary based on application requirements. While advanced methods like zero-crossing detection (ZCD), artificial neural networks (ANN), adaptive linear neurons (ADALINE), fundamental component extraction, and unit vector generation have emerged, this paper focuses on the widely used phase-locked loop (PLL) technique. PLL serves as the core synchronization controller, enabling fast and precise alignment between grid-interfaced converters and the utility network to extract or achieve the monitoring of the grid voltage information [7].

The PLL is important to respond to any variations in the grid voltage, like changes in power network configuration, which accordingly causes high utility voltage distortion with a great influence on harmonic amplification, and then is classified as a weak grid, thereby the quality of the power is disturbed. This, in turn, adversely impacts the power quality of the utility network and introduces various PQ issues into the distribution network. To prevent this, with the design stage of harmonic filters, utility characteristics should be considered. Therefore, in this paper, the effect of the voltage variation of the AC grid and the harmonic phenomenon is investigated [30,31]. The performance of PLL systems becomes particularly crucial during abnormal grid conditions, including balanced/unbalanced faults, frequency/phase variations, and harmonic distortions.

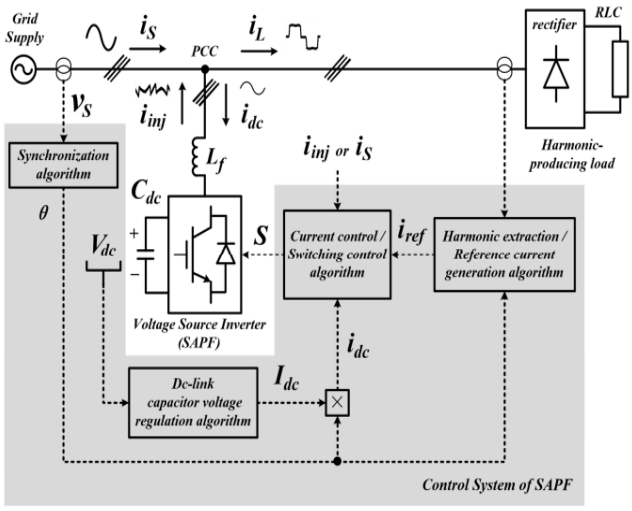

Fig. 2. SAPF associated with synchronization algorithm in its control system.

While numerous PLL techniques exist for phase angle estimation at the PCC, the most widely adopted conventional methods remain the abc-PLL, αβ-PLL, and dq-PLL, all of which rely on the fundamental positive-sequence component of grid voltage. An effective PLL design must therefore ensure robust operation under grid disturbances, delivering fast dynamic response, minimal oscillation/overshoot, and low computational burden for practical real-time implementation. For SAPFs, the control strategy must address all current harmonics, even when the supply voltage contains not only positive-sequence components but also negative- and zero-sequence harmonics. This necessitates a PSD to accurately extract the amplitude, phase angle, and frequency of the fundamental positive-sequence voltage (V^{+1}) as instantaneous values [32, 33]. In this context, this paper introduces an abc-PLL system that utilizes the fundamental PSD of grid voltage for enhanced synchronization accuracy.

As established in prior discussions, SAPF design revolves around four critical control domains: (1) controlling of current reference generation or harmonic extraction; (2) controlling of DC-link capacitor voltage (Vdc); (3) controlling of switching pulses; (4) controlling of synchronization. The overall performance of SAPFs is fundamentally governed by both the efficacy of these control algorithms and the careful selection of system parameters. Key design elements, including PI controller gains (Kp, Ki), DC-link capacitance (Cdc), and coupling impedance values of SAPFs (Rc, Lc), significantly influence filter effectiveness. Achieving optimal SAPF operation necessitates precise optimization or selection of these parameters to ensure optimal compensation performance [34,35].

Previous research has explored various optimization approaches for SAPF parameters. Taguchi's signal-to-noise ratio (SNR) method was compared with genetic algorithms (GA) for comprehensive parameter optimization in [34]. Study [35] introduced the novel nm-Predator Prey Fire-Fly algorithm (nm-PPFO) specifically for SAPF tuning. For DC bus voltage control, research [36] demonstrated the

superiority of interval type-2 fuzzy logic systems (T2FLS) over conventional type-1 systems (T1FLS). The Enhanced Artificial Bee Colony Algorithm (EABC) was employed in [37] to optimize PI controller gains in single-phase SAPFs.

Additionally, work [38] presented a hybrid PSODE algorithm, offering a comparative analysis against standard particle swarm optimization (PSO) and differential evolution (DE) methods for PI controller tuning. Also, DC-link voltage regulation in SAPFs has been addressed through multiple control strategies. Study [39] compares traditional PI controllers with neural network alternatives, whereas [40] employs the water cycle algorithm (WCA) to optimize both standard PI and fractional-order PI (FOPI) controllers. Further advancing this field, [41] implements PSO for precise tuning of PI controller gains, resulting in enhanced dynamic response and improved voltage regulation performance. Also, a variety of optimization methods have been explored in this brief literature review, shown in Table 1, to emphasize the great importance of the optimizer in reaching an effective PI-Controller for both the PLL synchronization circuit and a DC link voltage regulator circuit.

This research leverages the Dandelion Optimizer (DO) metaheuristic algorithm for optimization tasks. Through extensive benchmarking against leading optimization methods, including the Aquila Optimizer (AO), Mayfly Optimization Algorithm (MOA), and War Strategy Optimizer (WSO), the study demonstrates DO's superior capability in achieving diverse objective functions.

The motivations and contributions of this paper are:

- For the first time, the Dandelion Optimizer (DO), a recently developed metaheuristic algorithm, is applied to address a real-world power quality problem, specifically in optimizing SAPF controller parameters within smart grid systems.
- This research assesses the work in two directions, in addition to minimizing the THD. The first part examines the influence of conventional and adaptive controllers, whereas the second part discusses and compares the different recent optimization techniques.
- The study incorporates smart grid concepts such as self-monitoring, adaptive power networks, and advanced control technologies aimed at improving power quality, reducing system losses, and enhancing grid resilience against disturbances.
- The proposed optimization based SAPF control strategy is tested under a wide range of practical operating conditions, including grid voltage distortion, unbalanced utility voltages, and dynamic load variations, within a single, unified framework using soft computing approaches.

Table 1. Brief literature review

Reference	Contribution	Year
[42]	This study investigates the effectiveness of a PV-based shunt active power filter with nonlinear loads in reducing harmonic distortion and improving overall power quality. The proposed configuration of PV-SAPF incorporates a biogeography-based optimization (BBO) tuned PI controller for DC-link voltage control, and operates under ideal voltage conditions.	**[2023]**
[43]	This study proposes an intelligent tuned PQ control theory for SAPF and introduces an analysis of intelligent tools based on different Differential Evolution (DE) techniques, leading to optimal tuning of PI controller gain values for harmonic reduction and power quality improvement.	**[2023]**
[44]	This paper is a proposal for an estimator of the Hybrid Active Power Filter (HAPF) parameter accurately. For evolving this estimator, an objective function that mathematically embeds filter parameters and harmonic pollution is presented based on using the Amended Crow Search Algorithm (ACSA).	**[2023]**
[45]	This study deals with the application of three-dimensional fuzzy logic to DC voltage regulation in active power filters exploration in power quality improvement of PV smart grid system installation.	**[2023]**
[46]	This study introduces a novel Artificial Bee Colony-based optimized Artificial Neural Network (ABC-ANN) algorithm for the purpose of improving the power quality in a SAPF-based power system. Firstly, the PSO technique is used to tune a standard PI controller to its optimum gain values (Kp, Ki). Then, supply these inputs to the ANN controller. To find the optimal weight, this ANN controller has been tuned with the ABC algorithm.	**[2023]**
[47]	In this paper, a proportional-integral (PI) control unified power quality conditioners with distributed generation (UPQC-DG) system is optimized for stabilizing the DC link voltage fluctuations using an innovative real-time Particle Swarm Optimization (PSO) tuning approach.	**[2024]**
[48]	In this paper, the improvement of power quality (PQ) in a distribution system using a PV-SAPF is investigated. The performance of the proposed filter is increased using an enhanced Jaya optimized proportional integral (PI) with an indirect current controller (ICC) technique.	**[2024]**
[49]	This paper introduces the Golden Jackal Optimizer (GJO) incorporates an optimized PI controller for DC-link voltage regulation and an optimized output filter in SAPF to enhance the system quality.	**[2025]**
[50]	In this paper, a PV-fed unified power quality conditioner UPQC with an Adaptive Lizard Algorithm (ALA) is introduced. The ALA-based PI controller is designed to generate the parameters of Kp and Ki and maintain a constant DC link voltage of the UPQC for the elimination of harmonics.	**[2025]**
[51]	This paper proposes a novel PI tuning approach based on the Pity Beetle Algorithm (PBA) for enhancing the performance of the SRF-PLL grid synchronization system for grid-connected power converter applications. The proposed method is thoroughly assessed under challenging grid abnormalities.	**[2025]**

➢ The results demonstrate the effectiveness of the proposed method in significantly reducing THD, while ensuring stable DC-link voltage regulation and achieving fast dynamic response and convergence speed under various grid conditions.

➢ The performance of the proposed methodology is validated through a detailed MATLAB/Simulink-based test system. Comparative analysis against other published optimization techniques confirms the superiority of the DO-based approach in terms of current harmonic mitigation, control stability, and dynamic performance.

This paper is structured as follows: Section 2 outlines the proposed control system architecture for the SAPF. The configuration and parameters of the SAPF are detailed in Section 3. Section 4 presents the problem definition and the objective function. The optimization algorithm parameters are discussed in Section 5. Section 6 covers Proposed Methodology, Section 7 illustrates the simulation results and their analysis for the proposed optimization methods. Finally, Section 8 provides the conclusion.

2. Proposed Control System of SAPF

To finalize the three-phase SAPF model depicted in Figure 2, the control strategy hinges on four core components: (a) DC-link voltage regulation, (b) reference current extraction, (c) current control, and (d) synchronization algorithms. The control block diagram is shown in Figure 3, [28,52].

2.1. DC-Link Voltage Control Algorithm

Figure 3a shows a dynamic voltage regulation mechanism where the system compares the measured DC-link capacitor voltage (V_{dc}) against its desired reference value ($V_{dc,ref}$). to produce a voltage error $e(t)$ that serves as the critical input to the PI-controller at each sampling instant, as formulated in Eq. (1). The sophisticated PI-controller, with its transfer function $H(S)$ Indicted in Eq. (2), the expert calculates the required reference current magnitude ensuring optimal DC-link capacitor voltage. The controller's output represents the peak value of the reference supply current ($I_{max} = I_{sm,ref} = I_{Sm}{}^{*}$) as indicated in Eq. (3) [52].

$$e(t) = V_{dc,ref} - V_{dc} \tag{1}$$

$$H(S) = K_P + \frac{K_i}{S} \tag{2}$$

$$I_{Sm}{}^{*} = k_p\, e(t) + k_i \int_0^1 e(t)\, d(t) \tag{3}$$

In this control setup, the proportional gain (k_p) shapes the DC-link voltage response, while the integral gain (k_i) speeds up settling and completely eliminates steady-state voltage errors. These gains are set by mathematical or heuristic methods, and their values are mathematically derived from Eq. (4) and Eq. (5) [52].

$$k_p = 2.\zeta.\omega_n.C \tag{4}$$

$$k_i = {\omega_n}^2.C \tag{5}$$

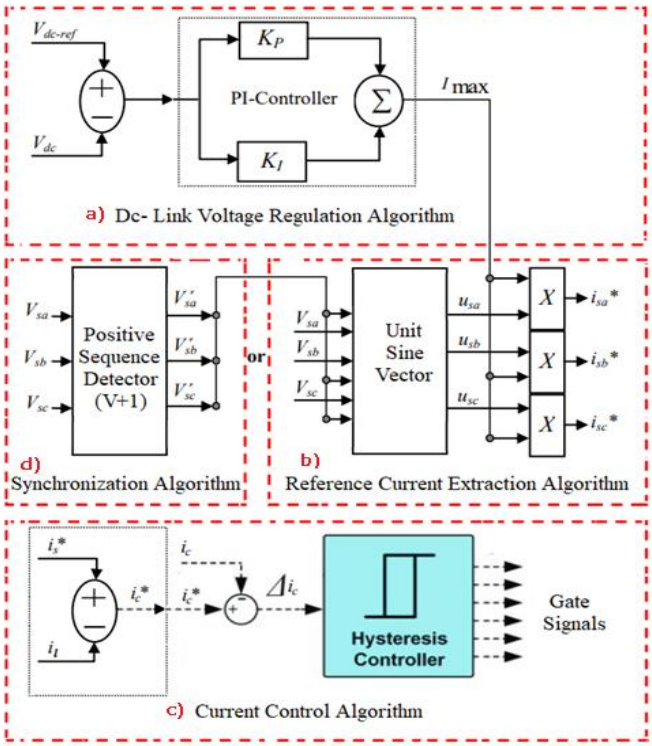

Fig. 3. The block diagram for the SAPF control strategy.

where, C - dc-link capacitor value, $\zeta = \frac{\sqrt{2}}{2}$ - damping factor, and ω_n - natural frequency, chosen as the supply fundamental frequency. As main part of the objective functions of the proposed optimization algorithms in this study is to optimally tune the PI-controller gains for the DC-link voltage regulator.

2.2. Reference Current Extraction Algorithm

As illustrated in Figure 3b, the unit sine vector templates are generated by sensing the instantaneous supply voltages, as mathematically expressed in Eq. (6) [35,37]:

$$V_s = \begin{cases} V_{sa} = V_{sm}\, sin(\omega t), \\ V_{sb} = V_{sm}\, sin(\omega t - 120^o), \\ V_{sc} = V_{sm}\, sin(\omega t + 120^o), \end{cases} \tag{6}$$

where, V_{sm} - represents the source voltage peak value, $\omega = 2\pi f$ - fundamental angular frequency.

To achieve a harmonic-free unity power factor, the three-phase source currents are estimated using unit sine vector templates. These templates align precisely with the source voltages and their peak values. The derivation of the unit sine vector templates is given in Eq. (7) [35,37]:

$$u_s = \begin{cases} u_{sa} = V_{sa}/V_{sm} = sin(\omega t), \\ u_{sb} = V_{sb}/V_{sm} = sin(\omega t - 120^o), \\ u_{sc} = V_{sc}/V_{sm} = sin(\omega t + 120^o), \end{cases} \tag{7}$$

In steady-state, the unit sine vector template maintains a unity amplitude. However, during transient conditions, its amplitude varies in response to load changes. The output of these templates is then multiplied by the PI controller's output, scaled to the peak amplitude of the estimated reference current ($I_{Sm}{}^{*}$), generating the required reference

currents ($I_{s,ref} = I_S{}^*$), as detailed in Eq. (8) and Eq. (9) [28],[35],[37],[52]:

$$I_S{}^* = I_{s,ref} = I_{Sm}{}^* . u_s \quad (8)$$

$$I_S{}^* = \begin{cases} I_{sa}{}^* = I_{Sm}{}^* \sin(\omega t) \ , \\ I_{sb}{}^* = I_{Sm}{}^* \sin(\omega t - 120^o) , \\ I_{sc}{}^* = I_{Sm}{}^* \sin(\omega t + 120^o), \end{cases} \quad (9)$$

2.3. Current Control Algorithm

The PWM current controller critically defines SAPF performance by producing optimal VSI gating signals from reference current estimates. Owing to its fast response, stability, accuracy, and simplicity, the HCCT is proposed as the optimal control method for enhanced SAPF performance [28,52].

As depicted in Figure 3c, the filter reference current ($I_C{}^*$) is derived from the sum of the measured load current (I_l) and the extracted supply current reference ($I_S{}^*$), as formulated in Eq. (10). This reference current, along with the VSI output current, is then processed by the model predictive current controller to generate optimal gating signals for the SAPF using HCCT [28,37].

$$I_C{}^* = I_S{}^* - I_l \quad (10)$$

2.4. Synchronization Algorithm

Figure 3d presents the proposed synchronization algorithm incorporating a (PSVD) that generates balanced sinusoidal voltage templates ($V_{Sa}{}'$, $V_{Sb}{}'$, and $V_{Sc}{}'$) from potentially distorted or unbalanced supply voltages ($V_{sa}, V_{sb}, and\ V_{sc}$). Theoretically, this control part is ineffective with ideal supply voltages, and only in this case can you skip it and directly apply the control part in Figure 3b, but realistically, the source voltage is not considered ideal and therefore cannot be dispensed with before applying the control part in Figure 3b. While the SAPF is designed to compensate for all current harmonics, the supply voltage typically contains a dominant positive-sequence component along with possible negative and zero-sequence harmonics. This necessitates the inclusion of a positive-sequence detector in the filter architecture to accurately extract the fundamental positive-sequence voltage (V^{+1}) parameters, enabling accurate control even under distortion, using dual p-q theory and a robust PLL circuit with a PI-controller. Figure 4 shows the PLL control block diagram, highlighting the PI-controller as a critical element for achieving the paper's objectives through optimization of its gains using the proposed algorithms [30-32].

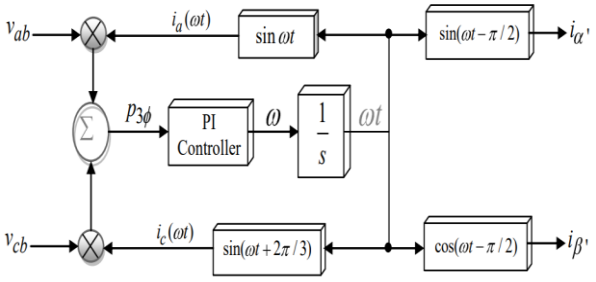

Fig. 4. Control block diagram for the PLL circuit.

3. System Configuration and Parameters of SAPF

The proposed configuration model, shown in Figure 5, consists of a grid-connected AC power system interfacing with an inductive nonlinear load. The load is connected on the DC side via an uncontrolled full-bridge diode rectifier. At the Point of Common Coupling (PCC), a Shunt Active Power Filter (SAPF) is integrated, which is connected to a DC-link bus capacitor through a Voltage Source Inverter (VSI). These components form the complete model under study. The selection of SAPF parameters is of utmost importance. Coupling inductor L_f, dc side capacitor C_{dc}, and dc reference voltage $V_{dc,\ ref}$ can be chosen assuming: 1) proper sinusoidal source current; 2) the maximum distortion allowed for the AC line current must be within 5%, and 3) the inverter operates in a linear modulation mode. The parameters coupling inductor L_f and the DC capacitor C_{dc} can be fetched as follows.

3.1. Selecting the DC Bus Voltage

The system's energy source is the DC storage capacitor, carefully sized to let the controller track the reference signal effectively. The DC-link voltage (V_{dc}) is determined based on the minimum voltage needed at the VSI output and must be nearly twice the supply phase voltage peak to ensure full-range operation. Consequently, the minimum DC-link voltage($V_{dc,min}$), is fundamentally dependent on the system's line voltage, and the required V_{dc} for the VSI can be expressed mathematically as formulated in Eq. (11) as follows [38,39,41,53,54]:

$$V_{dc,min} = \frac{2\sqrt{2}\ (V_{LL,rms})}{\sqrt{3}(m)} \quad (11)$$

Where, $V_{LL,rms}$ Is the line-to-line RMS voltage at PCC, m is the modulation index (selected as 1), and therefore, with a $V_{LL,rms}$ Of 380 V, the magnitude of V_{dc} is calculated as 620.5 V, and it is selected and fixed at 650 V as a reference value.

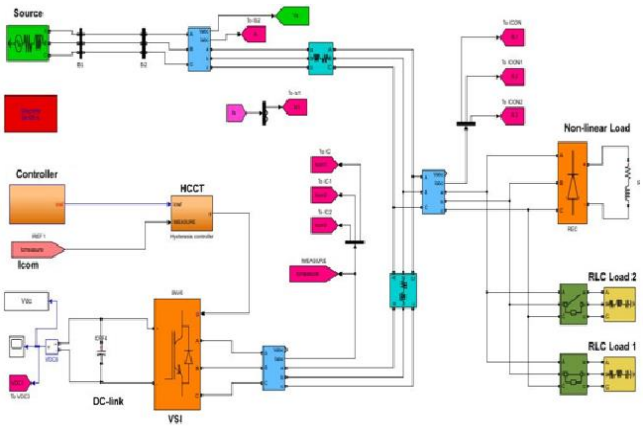

Fig. 5. MATLAB/Simulink model for the proposed configuration system.

3.2. Selection of the DC Bus Capacitor

The DC bus capacitor (C_{dc}) is designed to maintain voltage stability during load transients, compensating for

both voltage sags during sudden load application and surges during load removal. Its capacitance must be precisely calculated to ensure sufficient energy storage capacity for instantaneous real power exchange, enabling the SAPF to meet dynamic load requirements. Furthermore, under unbalanced operating conditions where harmonics appear in the DC bus voltage, the capacitor must provide effective harmonic suppression. The design of C_{dc} is expressed by Eq. (12) [38,41,53]:

$$C_{dc,min} = \frac{3.V_{Ph}.i_{sh}.a_f.k_e.t}{1/2(V^2{}_{dc,ref} - V^2{}_{dc,min})} \quad (12)$$

In this formula, V_{Ph} represents the phase voltage, i_{sh} denotes the phase current handled by the SAPF, a_f The overloading factor, and t refers to the time required to reach steady-state operation. The parameter k_e captures the energy variation under dynamic conditions, while $V_{dc,ref}$ and $V_{dc,min}$ Indicate the reference and minimum required DC-link voltages, respectively. Based on the system parameters, the calculated values are, $V_{dc,min}$=620.5V, $V_{dc,ref}$=650V, V_{Ph}= 220 V, i_{sh}= 10 A, t = 50 m sec, a_f= 1.2, and k_e = 0.1 (reflecting a 10% dynamic energy variation).The value of $C_{dc,min}$ Is calculated as 2.1 mF. For practical implementation, this value is rounded and approximated to 2 mF.

3.3. Choosing a Filter Inductor

The interface inductor L_f is crucial to SAPF performance, with its design directly impacting the system's ability to deliver clean and accurate current compensation. Its value balances filter current ripple reduction with efficient high-frequency switching. A properly selected inductor ensures that the VSI can track the reference current with high precision. When paired with a sufficiently high DC-link voltage, a well-sized inductance significantly boosts compensation performance. To maximize the inductor's effectiveness, the switching frequency is also pushed to its optimal upper limit, ensuring a responsive and smooth dynamic behavior. The SAPF is integrated into the power network via an interface inductor, which functions as a passive filter whose performance is directly influenced by the switching frequency. The ripple current ($I_{cr,pp}$) serves as a critical parameter in determining the inductor's effectiveness. The design equation for calculating the optimal inductance value is expressed in Eq. (13) as follows[41,53,54]:

$$L_{f,min} = \frac{\sqrt{3}.m.V_{dc,ref}}{12.a_f.f_{SH}.I_{cr,pp}} \quad (13)$$

Based on the selected design parameters, $I_{cr,\,pp}$ set at 8% of the phase current (defined as 10% of the RMS phase current handled by the SAPF), f_{SH} of 10 kHz, modulation index (m) equal to 1, $V_{dc,ref}$ of 650 V, and an a_f of 1.2, the required minimum interfacing inductance ($L_{f,min}$) is calculated to be 1 mH. Accordingly, a practical value of 1 mH is chosen and implemented in this investigation to ensure reliable and efficient filter performance.

3.4. System Parameters of SAPF

The device parameters selected to implement the proposed system are indicated in Table 2, providing a clear overview of the key specifications utilized in this study.

Table 2. Proposed system parameters

Device	Parameters	Values
Supply Parameters	Frequency f_s	50 Hz
	Voltage V_s	380 V
	Source line inductor L_s	2 mH
	Source line resistor R_s	4 Ω
Non-Linear Load	Load inductor L_{dc}	30 mH
	Load resistor R_{dc}	4 Ω
SAPF Parameters	Interface inductor L_f	1 mH
	Interface resistor R_f	0.5 Ω
	DC side capacitor C_{dc}	2 mF
	References voltage $V_{dc,\,ref}$	650 V

4. The Problem Definition and Objective Functions

The proposed optimization algorithms aim to fine-tune the PI-controller gains (K_p and K_i) for both PLL and DC-link voltage regulation in adaptive and conventional SAPF controllers. This tuning process is designed to accomplish several key objectives, including eliminating steady-state errors in the PI controllers and minimizing the total harmonic distortion of the source current (THDi). These improvements adhere to stringent harmonic standards such as IEEE 519-1992 [55], IEEE 519-2014 [56], and IEEE 519-2022 [57], which require maintaining THD below 5% to enhance the PQ and reduce harmonic interference in contaminated power systems. As shown in Figure 6, the optimization process systematically adjusts the controller gains (K_p and K_i) to meet these objectives effectively and efficiently [30,31,58].

The THDi represents the quantitative measure of harmonic pollution, calculated as the RMS ratio of all harmonic components (up to a specified order) to the fundamental frequency component, as defined in Eq. (14). In this context, the proportional gain (K_p) primarily addresses instantaneous system errors, while the integral gain (K_i) eliminates steady-state deviations. The PI controller's complete mathematical representation comprises its transfer function. $G_c(s)$ in Eq. (15) (frequency domain) and the time-domain output signal $u(t)$ In Eq. (16), providing a comprehensive characterization of the control dynamics [30,31,58]:

$$THD_i = \sqrt{\frac{\sum_{k=2}^{k_{max}} I_k^2}{I_1^2}} \quad (14)$$

$$G_c(s) = k_p + \frac{k_i}{s} \quad (15)$$

$$u(t) = e(t) + k_i \int_0^1 e(t)\, d(t) \quad (16)$$

where, $e(t)$ Is the error between the actual and reference DC bus voltage (V_{dc}, $V_{dc,\,ref}$), respectively.

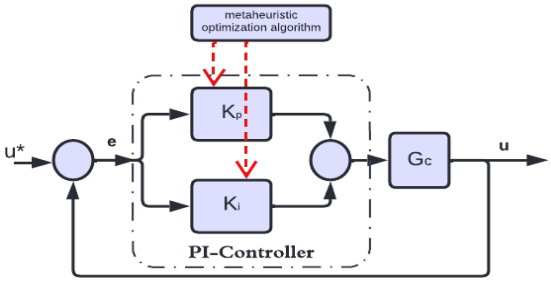

Fig. 6. PI-controller control system using optimization algorithms.

5. Dandelion Optimizer

The Dandelion Optimizer (DO) is a swarm intelligence algorithm inspired by the wind-dispersed flight of dandelion seeds [59, 60]. It employs a dual-group strategy (core and assistant dandelions) and distinct seed-sowing mechanisms to effectively balance global exploration and local convergence, preventing premature convergence in complex optimization tasks. It evolves through four key phases:

- *Step 1: Initialization*

In the DO algorithm, each seed represents a potential solution within the search space. The collective set of these candidate solutions forms the population of the algorithm, which is mathematically represented in Eq. (17).

$$X_i = LB + rand \times (UB - LB) \quad (17)$$

Here, i is an integer ranging from 1 to the total population size, and $rand$ denotes a random number between 0 and 1. The upper and lower bounds (UB and LB) are defined as follows: $LB = [lb_1, lb_2, \ldots\ldots, lb_{Dim}]$ and $UB = [ub_1, ub_2, \ldots\ldots, ub_{Dim}]$.

The initial elite individual in the DO algorithm is the solution with the highest fitness value, representing the optimal position for dandelion seeds in the search space. For minimization objectives, this elite solution is identified and preserved during initialization using Eq. (18) and Eq. (19):

$$f_{best} = min(f(X_i)) \quad (18)$$

$$X_{elite} = X(find(f_{best} == f(X_i))) \quad (19)$$

- *Step 2: Rising*

Dandelion seeds must reach a sufficient height to ensure successful dispersal from the parent plant. The initial ascent of dandelion seeds, influenced by environmental factors like wind and humidity, is modeled by Eq. (20) and Eq. (21) to determine their upward trajectory.

$$X_{t+1} = \begin{cases} X_t + \alpha \times v_x \times v_{y\times} \ln Y \times (X_s - X_t), randn < 1.5 \\ X_t \times k \quad , else \end{cases} \quad (20)$$

$$X_s = LB + rand \times (UB - LB) \quad (21)$$

Where, at iteration t, X_s represents a randomly chosen position, while X_s Indicates the position of the dandelion seed at the same iteration. The term $\ln Y$ follows a lognormal distribution with parameters $\mu = 0$ and $\sigma^2 = 1$, as given in Eq. (22).

$$\ln Y = \begin{cases} \frac{1}{y\sqrt{2\pi}} exp[-\frac{1}{2\sigma^2}(\ln y)^2], & y \geq 0 \\ 0 \quad , & y < 0 \end{cases} \quad (22)$$

where the standard normal distribution variable $y \sim N(0,1)$ provides controlled stochasticity for the algorithm's exploration phase. The parameter α denotes a random variable within the range [0, 1], introducing controlled stochastic perturbations. Meanwhile, v_x and v_y Represent the lift coefficient components of the dandelion seed, and θ serves as a random angular variable within the bounds of [-π, π], enabling omnidirectional exploration in the search space. Each can be computed as expressed as follows:

$$\alpha = rand \times \left(\frac{1}{T^2}t^2 - \frac{2}{T}t + 1\right) \quad (23)$$

$$r = \frac{1}{e^{\theta}} \quad (24)$$

$$v_x = r \cos\theta \quad (25)$$

$$v_y = r \sin\theta \quad (26)$$

$$k = 1 - rans \times q \quad (27)$$

$$q = \frac{1}{T^2-2T+1}t^2 - \frac{1}{T^2-2T+1}t + 1 + \frac{1}{T^2-2T+1} \quad (28)$$

- *Step 3: Descending*

During this stage, dandelion seeds rise and then descend gradually, representing the exploration phase. The DO algorithm simulates this motion using Brownian movement to mimic the seeds' natural drifting path.

$$X_{t+1} = X_t - \alpha \times \beta_t \times \left(X_{mean,t} - \alpha \times \beta_t \times X_t\right) \quad (29)$$

- *Step 4: Landing*

The DO enters its final exploitation phase, where it strategically refines the search to converge on optimal solutions. Each dandelion seed's final position is determined through an adaptive probability mechanism that balances previous search knowledge with controlled randomness. This process ensures steady convergence toward the global optimum, where refined adjustments lead to the most effective solution, mathematically expressed as follows:

$$X_{t+1} = X_{elite} + levy(\lambda) \times \alpha \times (X_{elite} - X_t \times \delta) \quad (30)$$

$$levy(\lambda) = s \times \frac{\omega \times \sigma}{\frac{1}{|t|^{\beta}}} \quad (31)$$

$$\sigma = \left(\frac{\Gamma(1+\beta)\times sin\left(\frac{\pi\beta}{2}\right)}{\Gamma\left(\frac{1+\beta}{2}\right)\times sin\left(\frac{\beta-1}{2}\right)}\right) \quad (32)$$

$$\delta = \frac{2d}{T} \quad (33)$$

Here, X_{elite} Represents the optimal position of the seed, while s is a fixed constant set to 0.01. The parameter β is a randomly generated value ranging between 0 and 2, and both d and ω are arbitrary numbers selected within the interval [0, 1]. A comprehensive flowchart illustrating the DO algorithm's architecture is presented in Figure 7. The suggested parameters for the selected optimization algorithms are presented in Table 3.

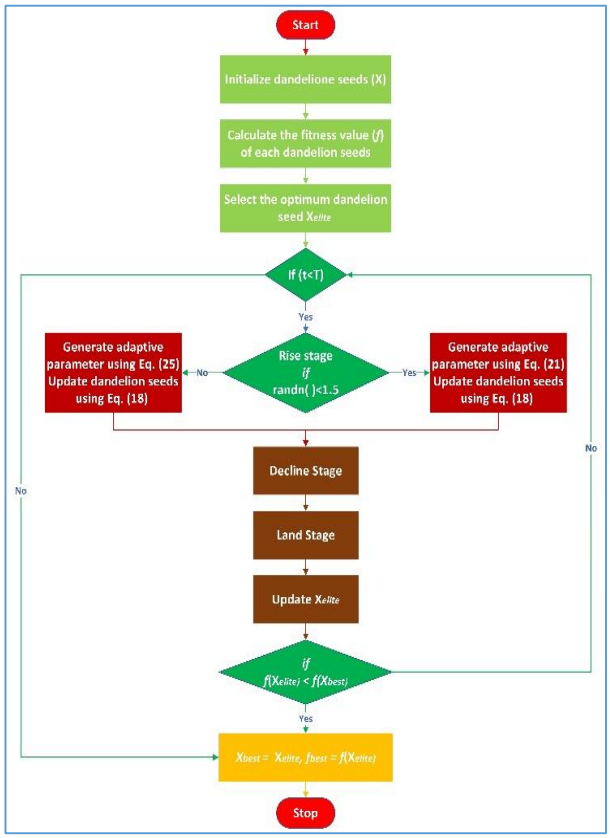

Fig. 7. Flowchart of the DO algorithm.

Table 3. Optimization algorithm parameter settings

Algorithm	Parameters	Values
AO	Iterations Maximum Number	200
	r_1	10
	U	0.0265
	ω	0.005
	α	0.1
	δ	0.1
	β	1.5
DO	Iterations Maximum Number	200
	Population Count	50
	β	1.5
MOA	Iterations Maximum Number	200
	Population Count	50
	Inertia Weight	0.8
	Personal Learning Coefficient	1
	Inertia Weight Damping Ratio	1
	Global Learning Coefficient	1.5
	Distance Sight Coefficient	2
	Random flight	1
	Nuptial Dance	5
	Damping Ratio	0.8
	Number of Offspring	2
	Mutation Rate	0.01
WSO	Maximum Number of Iterations	200
	Population Size	50
	Exploration and exploitation parameter	0.1

6. Proposed Methodology

6.1. Proposed Controllers and Initialization Data

In this paper, MATLAB/SIMULINK is employed as a powerful simulation platform to implement and evaluate the proposed optimization techniques. The simulation environment enables detailed performance analysis of these competing approaches, providing critical insights into their dynamic behavior and operational effectiveness. The research uses simulations to critically assess two control techniques:

A. The first controller depends on a conventional controller technique.
B. The second controller depends on the adaptive controller technique.

All simulation results for the proposed controllers, along with the applied optimization algorithms, are executed within the MATLAB/SIMULINK environment. The initial parameter settings for the DO, AO, MOA, and WSO algorithms are detailed in Table 4, providing the foundation for consistent and accurate performance evaluation.

6.2. Simulation Scenarios

The purpose of the optimization process is to get the optimal values for the PI-controller gains to accomplish the objective functions. Then, the performance of the controllers is evaluated according to the following cases, which are explained as follows:

- **Case (A):** The system was simulated under an ideal source voltage condition without using the filter to observe the effect of the harmonic distortion before applying the proposed mitigation technique.
- **Case (B):** The system was simulated with a filter connection, and the connected SAPF was controlled using the conventional technique.
- **Case (C):** The system was simulated with a filter connection, and the connected SAPF was controlled using the adaptive technique.

For the cases (B and C), several steps and scenarios were applied as follows:

- Simulation with an **unoptimized controller** to observe the performance of the filter without optimization.
- Simulation with **optimized controller** gains using the proposed optimization algorithms, the results are compared in terms of total harmonic distortion values, controller performance, including its stability and steady-state errors, as well as its convergence characteristics, to observe and choose the best optimization algorithm.
- Finally, the **best-proposed optimization algorithm** was chosen, and then it was applied to observe and assess the effectiveness of the optimized controller under the conditions of ideal and distorted supply voltage, as well as the variable or dynamic load conditions.

Table 4. Preliminary data for suggested optimization algorithms

No. of Variables	Variables Upper / Lower Limits				Objective functions		Population Number	Max. Iteration Number
	PI-Controller (1) gains		PI-Controller (2) gains		THD_i	SS-Error		
4	$10 < Kp_1 < 50$	$1< Ki_1 < 10$	$0.1< Kp_2 < 2$	$1< Ki_2 < 35$	$0 < THD_i< 5\%$	$0 < Error < 5\%$	50	200

7. Simulation Results

7.1. Case (A): Simulation without SAPF Connection

In this case, the tested model is simulated under an ideal source voltage condition connected to the NLL. The filter is absent and not connected to the system to study and estimate the effect of the NLL on the source current waveform and the extent of the THD generated due to the linked NLL. The importance of this step lies in determining the extent of the improvement required to be achieved and the harmonics to be compensated through the chosen active filter. As illustrated in Figure 8, under ideal supply conditions, the three-phase source voltage maintains perfect sinusoidal waveforms. However, when nonlinear loads are introduced without filtering, significant distortion becomes evident in both load and source currents, transforming their waveforms into non-sinusoidal patterns. This harmonic distortion is quantitatively analyzed in Figure 9 through FFT spectrum analysis, revealing a substantial THD of 23.44% in the source current due to NLL effects.

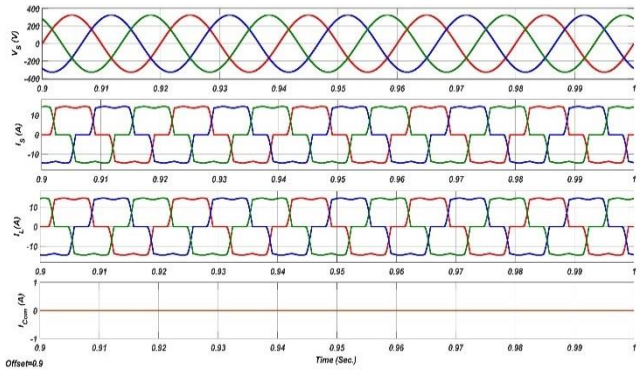

Fig. 8. Three-phase waveforms of source voltage and current in case (A) without SAPF.

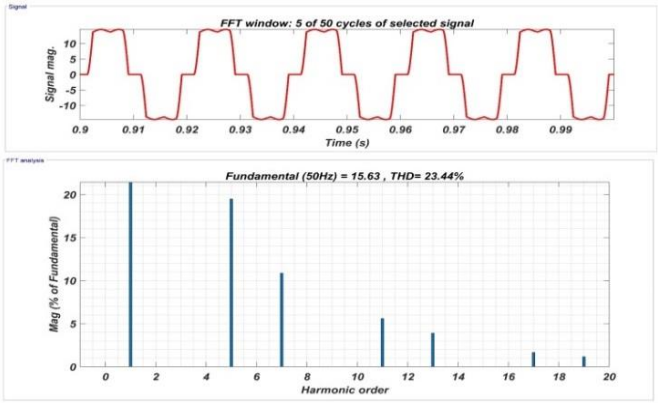

Fig. 9. Source Current waveform and its FFT harmonic spectrum without SAPF for case (A).

7.2. Case (B): Simulation with SAPF Controlled Using the Conventional Technique

In this case, SAPF is integrated into the system to reduce harmonic distortions in the source current caused by the NLL, with its operation controlled using a conventional technique. First, the controller is simulated without optimization, i.e., without tuning the PI controller gains, to appreciate the stability and response of the system before the optimization process. Then, optimization is done through an optimization proposed algorithm.

7.2.1. Simulation with an un-optimized conventional controller

In this scenario, the system was simulated without any optimization. Despite encouraging results in Figure 10, and Figure 11, where the source current waveform returned to a clean sinusoidal shape and the THD dropped to 1.97% as calculated by FFT, Figure 12 reveals a significant shortcoming. The DC-link voltage fails to reach the 650V reference promptly, taking an excessive amount of time to approach it. This slow response indicates instability in the filter's performance, leading to overall unreliable results and a controller that reacts slowly to fluctuations in the network.

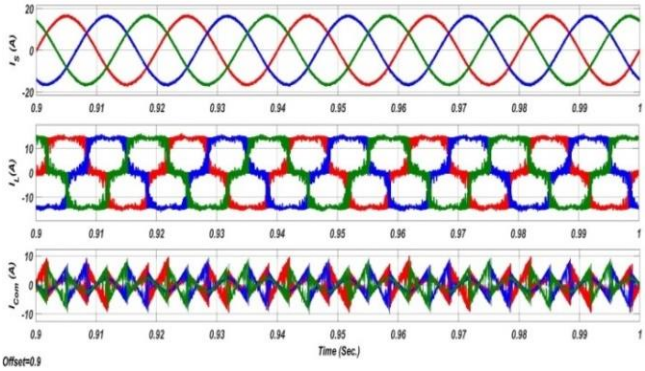

Fig. 10. Three-phase waveforms of source voltage and current with SAPF-controlled and un-optimized conventional controller for case (B).

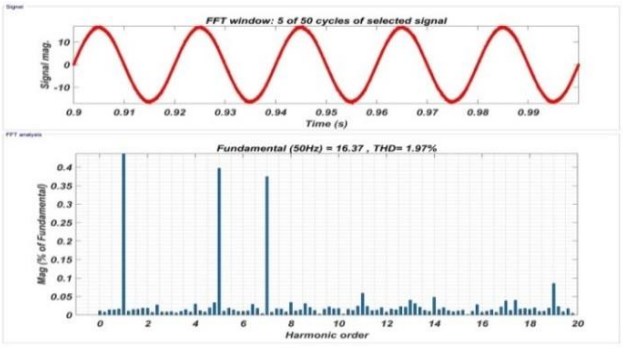

Fig. 11. Source Current waveform and its FFT harmonic with SAPF controlled and un-optimized conventional controller for case (B) .

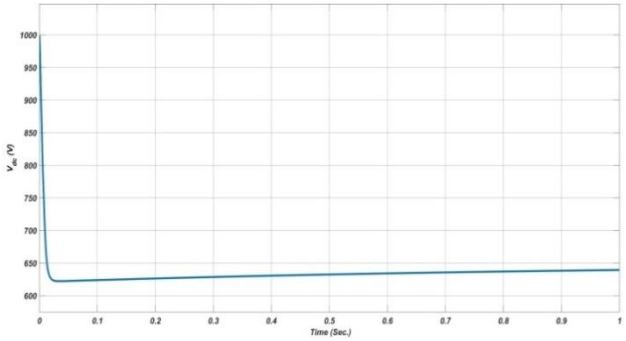

Fig. 12. Response of DC-link voltage value with its reference value for the SAPF controlled with an un-optimized conventional controller for case (B).

7.2.2. Simulation with an optimized conventional controller

In this scenario, the system was simulated with the SAPF controlled using both conventional methods and optimization algorithms for tuning the PI controller gains to enhance performance. Prior to implementation, a comprehensive comparative assessment of multiple optimization algorithms is conducted. This evaluation aims to identify the most effective approach for enhancing controller performance, specifically targeting improvements in dynamic response, operational stability, and PQ regulation.

7.2.2.1. Comparative performance analysis of all proposed algorithms against the conventional controller

Figure 13 demonstrates the dynamic performance of DC-link voltage regulation across all implemented algorithms, showcasing their rapid tracking capability and precision in maintaining the reference value. Each optimization technique exhibits excellent transient response characteristics, including fast settling time, minimal voltage overshoot, and low steady-state error. These performance enhancements directly contribute to superior SAPF controller stability and PQ improvement.

Table 5, shows a comparison between the results obtained using the proposed algorithms .The comparison criterion is the best fitness value, which is represented by the sum of the THDi and the error (the difference between the DC reference value "650V" and the actual DC side voltage).

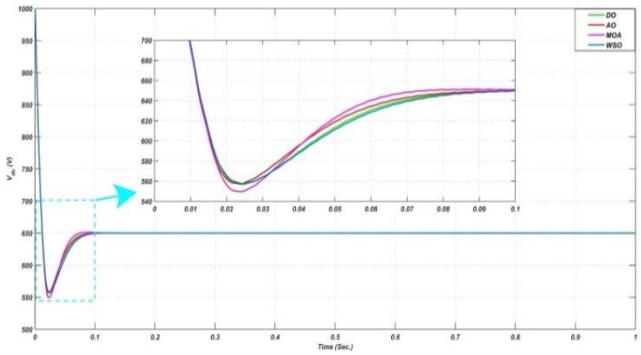

Fig. 13. Response of DC-link voltage values with their reference value for the optimization algorithms and the conventional.

Table 5. Optimized control solutions /parameters, THDi, and error fitness, and convergence iteration results for the optimization algorithms with the conventional controller for case (B)

Proposed tuning Algorithm	Best of fitness (%)	Corresponding		Best solutions		Convergence iteration
		THD	Error	K_p	K_i	
AO	2.0825	1.96	0.122	0.678	29.58	198
DO	2.076	1.95	0.126	0.6	24.938	160
MOA	2.0818	1.952	0.13	0.65	33.238	72
WSO	2.08	1.955	0.125	0.586	23.391	161

Minimizing these values is the objective function of the algorithms. The comparison was also made on the convergence of the algorithm to the best result in fewer iterations.

Table 5, and figure 14 show that the Dandelion Optimizer (DO) gives the best result in terms of Iterative convergence characteristics and the corresponding minimum THDi at the best solution values of control parameters/gains; Kp and Ki with values 0.6 and 24.938, respectively.

Also, figure 14 illustrates the iterative convergence characteristics of the objective function across four different optimization algorithms. Among them, the Dandelion Optimizer (DO) exhibits the fastest convergence rate, reaching the minimum objective function value in fewer than 70 iterations and stabilizing at approximately 2.076. In comparison, the WSO and MOA algorithms also achieve reasonable convergence, though at a slower pace and with more oscillations, stabilizing around 2.08 and 2.0818, respectively. The AO algorithm shows the weakest performance, maintaining a relatively high objective value (2.0825) and requiring a longer duration to reach steady state.

These results highlight the superiority of the DO algorithm in terms of both convergence speed and accuracy, making it well-suited for applications that demand fast response and precise control.

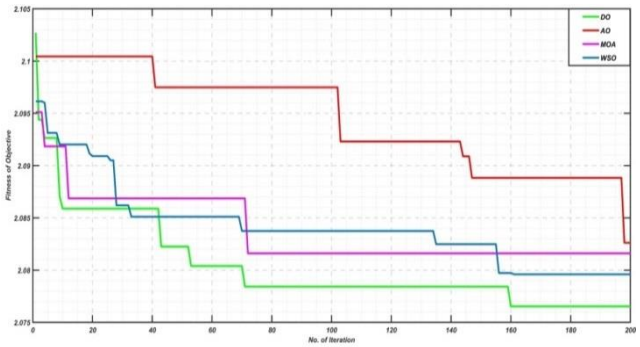

Fig. 14. Iterative convergence characteristics of the fitness function for the optimization algorithms, conventional controller for case (B).

It is clearly evident that the performance of the SAPF is greatly enhanced when optimization algorithms are used to tune the PI controller. With the application of optimized gains, the system achieves its best fitness by effectively minimizing the THDi objective function. Among the tested

algorithms, the DO algorithm stands out, delivering a best fitness value of 2.076% and achieving a THDi as low as 1.95%- the most optimal results compared to other algorithms. So, the conventional controller optimized using the DO algorithm is suggested to evaluate its performance under different conditions to show the extent of improvement and stability in SAPF performance with the proposed conventional controller.

7.2.2.2. Simulation with an optimized conventional controller using the DO Algorithm tested under ideal source conditions

In this scenario, the system was simulated under ideal voltage conditions, with a source waveform free from any distortions. Figure 15 displays the source voltage and current waves, both exhibiting pure sinusoidal waveforms, along with the load current and the filter's compensating current. Meanwhile, Figure 16 reveals a THD_i value of 1.95%, as determined through FFT harmonic spectrum analysis.

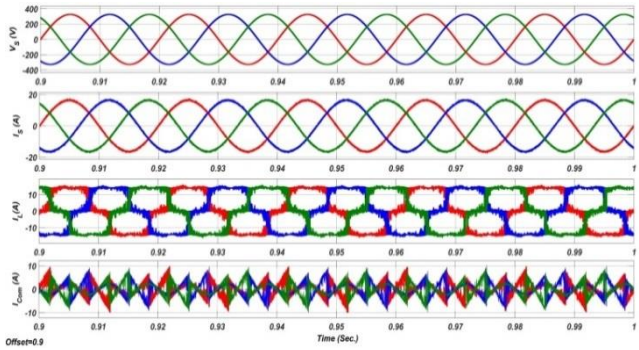

Fig. 15. Three-phase waveforms of source voltage and current with SAPF controlled with an optimized conventional controller using the DO algorithm and tested under ideal source conditions for case (B).

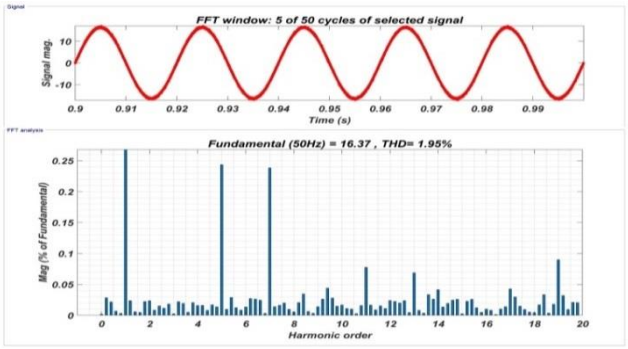

Fig. 16. Source Current waveform, and its FFT harmonic with SAPF controlled with optimized conventional controller using DO algorithm and tested under ideal source conditions for case (B).

7.2.2.3. Simulation with an optimized conventional controller using DO Algorithm tested under distorted source voltage conditions

The strong and distinctive performance of the controller appears when it is tested and evaluated with distortions in the supply voltage waveform. When the supply voltage is distorted by 8.05%, the THD for the supply current is maintained within a permissible value by the SAPF, which is controlled by the proposed optimized controller. Figure 17, illustrates the waveforms of the source voltage, source current, load current, and compensating current. Furthermore, Figure 18 presents the THD spectrum of the supply current, revealing a THD value of 2.99%.

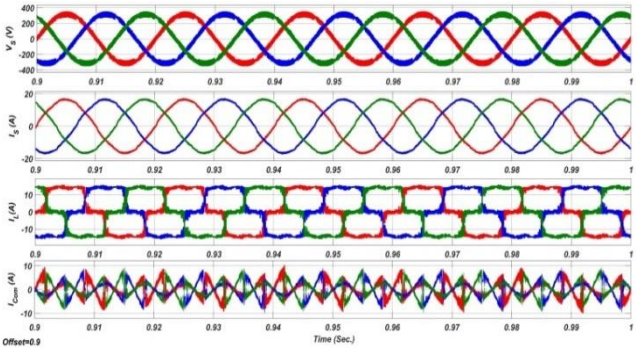

Fig. 17. Three-phase waveforms of source voltage and current with SAPF controlled with optimized conventional controller using DO algorithm and tested under distorted source voltage conditions for case (B).

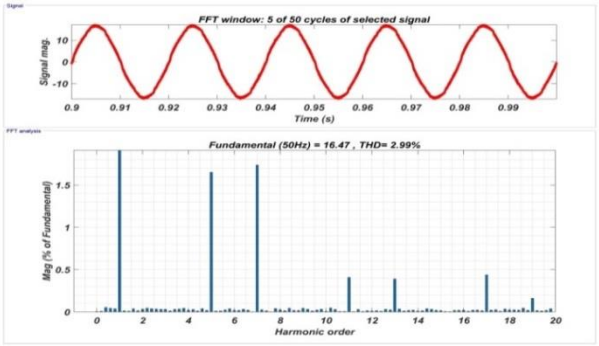

Fig. 18. Source Current waveform, and its FFT harmonic with SAPF controlled with optimized conventional controller using DO algorithm and tested under distorted source conditions for case (B).

7.2.2.4. Simulation with an optimized conventional controller using the DO Algorithm tested under load variation conditions

This section examines how the optimized controller performs amid dynamic changes and fluctuating load conditions. Where the system is overloaded by 150% of its rated values through connecting an RLC load in addition to the presence of an NLL. The RLC load was connected to the grid at 0.2 seconds into the simulation. Then disconnected at 0.4 seconds, as shown in Figure 19 where the supply current maintained its pure sinusoidal waveform. Figure 20 presents the FFT analysis results, revealing a THD_i of just 1.43% for the source current during the proposed overload interval under variable load conditions.

To thoroughly evaluate the controller's performance, it is essential to investigate how the DC-link voltage responds to varying load conditions. As shown in Figure 21, the dynamic response of the DC-link voltage closely follows its reference value despite fluctuations in load. The controlled SAPF maintains the voltage with minimal overshoot, low steady-state error, and rapid settling time, demonstrating a notable improvement in the dynamic performance of the SAPF controller.

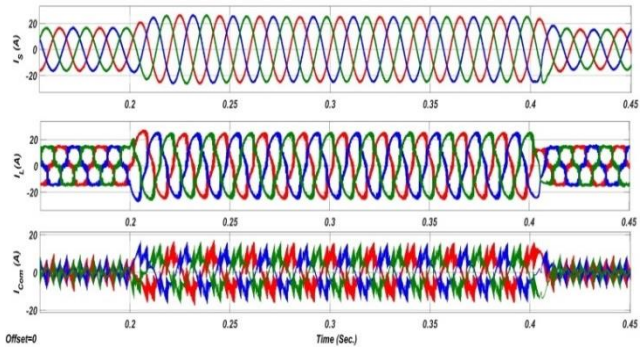

Fig. 19. Three-phase waveforms of source voltage and current with SAPF controlled with an optimized conventional controller using the DO algorithm and tested under load variation conditions for case (B).

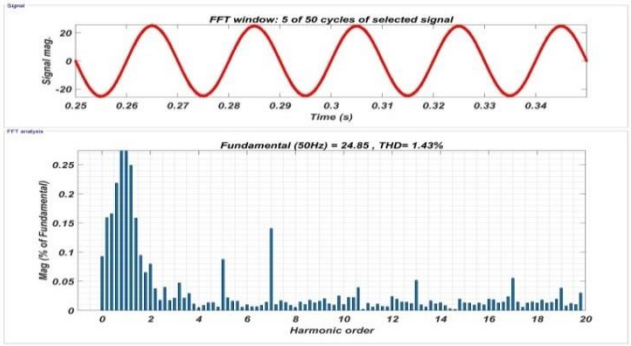

Fig. 20. Source Current waveform, and its FFT harmonic with SAPF controlled with optimized conventional controller using DO algorithm and tested under load variation conditions for case (B).

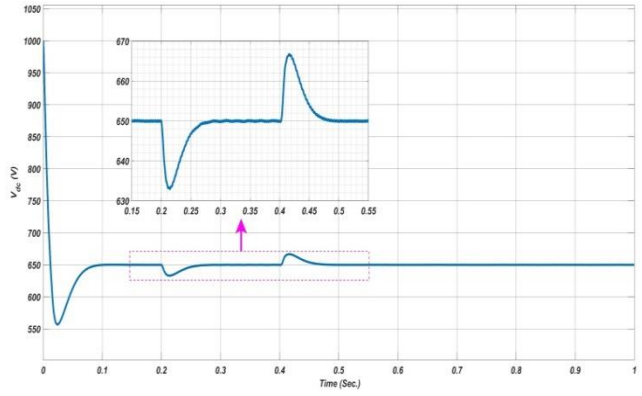

Fig. 21. Response of DC-link voltage of SAPF controlled with an optimized conventional controller using the DO algorithm, tested under load variation conditions for case (B).

It is observed that the conventional SAPF controller optimized with the DO algorithm yields acceptable values for the desired objective functions. This performance is consistent under various test conditions, including ideal and distorted source voltages, as well as dynamic load changes. Thus confirming the efficiency of the chosen DO optimizer.

7.3. Case (C): Simulation with SAPF controlled using the adaptive technique

In this case, SAPF is controlled by an adaptive technique to mitigate the harmonics produced by the NLL in the source current. Since the non-optimized scenario in this case is not much different from what was previously presented with the conventional controller, the discussion begins with the study of the proposed adaptive controller. This controller is simulated and optimized through the proposed optimization algorithms.

7.3.1. Simulation with an optimized adaptive controller

In this scenario, the system was simulated, and the SAPF was controlled by an adaptive technique. By using the optimization algorithms, the PI controller gains were tuned to enhance the controller's performance. The outcomes of the algorithms are compared to select the most effective algorithm for enhancing the controller's performance, response, and stability.

7.3.1.1. Comparison of the optimized outcomes for all proposed algorithms with the adaptive controller

As depicted in Figure 22, all implemented algorithms demonstrate exceptional tracking capability, with DC-link voltages rapidly converging to their reference values. The comparative analysis reveals consistently fast response times across all methods, along with favorable dynamic characteristics such as minimal settling time, acceptable overshoot, and negligible steady-state error. These features collectively enhance operational stability and ensure superior performance in the SAPF controller implementation.

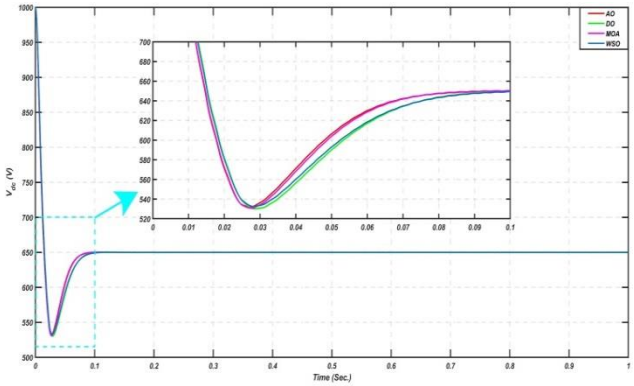

Fig. 22. The DC-link voltage response relative to its reference value for the optimization algorithms and the adaptive controller for case (C).

Table 6, shows a comparison between the results obtained using the proposed algorithms, where the comparison is made in terms of the best fitness, which is represented by the sum of the THDi and the error. Minimizing these values is the objective function of the algorithms. The comparison was also made on the convergence of the algorithm to the best result in fewer iterations.

Also, Table 6 and Figure 23 show that the DO algorithm gives the best result in terms of the best of fitness and the corresponding minimum THDi at the best solutions of

control parameters/gains; Kp_1, Ki_1, Kp_2, and Ki_2, with values given in Table 6. Figure 23, further emphasizes the long-term convergence behavior of the same algorithms, observed up to 200 iterations. The results confirm that the DO algorithm maintains its advantage by reaching the lowest objective value (2.087) before iteration 70 and remaining stable without oscillations throughout the optimization process. While the WSO and MOA algorithms also demonstrate steady convergence to approximately 2.0872 and 2.088, they experience intermittent stagnation during the optimization. AO continues to underperform, failing to reach comparable accuracy, which indicates its limited effectiveness in handling complex objective functions.

From a computational efficiency perspective, it can be concluded that the DO algorithm not only delivers accurate results but also achieves them in fewer iterations, reducing computational time and enhancing processing efficiency.

Table 6. Optimized control Solutions /parameters, THDi, and error fitness, and convergence iteration results for the optimization algorithms with the conventional controller for case (C)

Proposed tuning Algorithm	Best of fitness	Corresponding		Best solutions				Convergence iteration
		THD	Error	Kp_1	Ki_1	Kp_2	Ki_2	
AO	2.099	1.976	0.123	10	10	0.756	35	42
DO	2.087	1.958	0.129	25	1.14	0.61	25	52
MOA	2.088	1.963	0.125	27	2.92	0.72	33.27	78
WSO	2.0872	1.9622	0.125	42.72	6.6	0.636	25.77	61

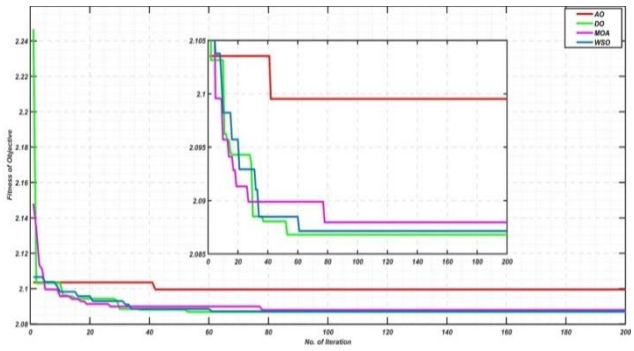

Fig. 23. Iterative convergence characteristics of the fitness function for the optimization algorithms with the adaptive controller for case (C).

7.3.1.2. Simulation with an optimized adaptive controller using the DO Algorithm tested under ideal source conditions

Following the same methodology as Case (B), this simulation examines system performance under ideal grid conditions with a completely undistorted source voltage. Figure 24 presents perfectly sinusoidal source voltage and current waveforms alongside the corresponding load current and active filter compensation current. The accompanying harmonic analysis in Figure 25 demonstrates outstanding performance, with FFT spectrum measurements revealing an impressively low THDi of merely 1.958% - clear evidence of excellent PQ.

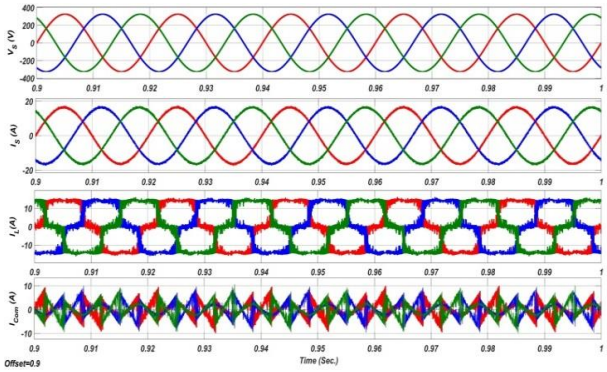

Fig. 24. Three-phase waveforms of source voltage and current with SAPF controlled with optimized adaptive controller using DO algorithm and tested under ideal source conditions for case (C).

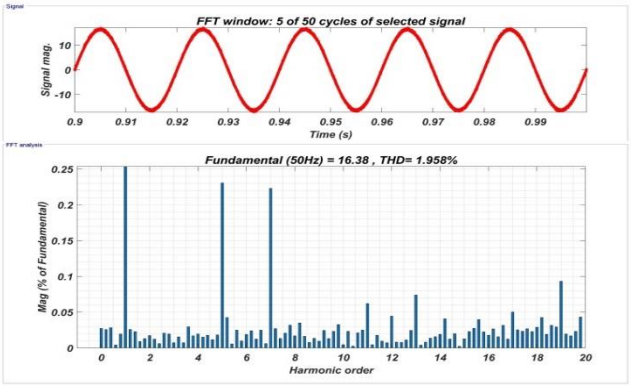

Fig. 25. Source Current waveform, and its FFT harmonic with SAPF controlled with optimized adaptive controller using DO algorithm and tested under ideal source conditions for case (C).

7.3.1.3. Simulation with an optimized adaptive controller using DO Algorithm tested under distorted source voltage conditions

The adaptive controller's robust performance and effectiveness of the optimizer technique appear and are demonstrated when tested and evaluated with distortions in the supply voltage waveform. When the supply voltage is distorted by 8.05%, the THD_i for the source current is maintained within the permissible value by the SAPF, which is controlled by the proposed optimized adaptive controller using the DO algorithm.

Figure 26 displays the waveforms of the source voltage and current, along with the load current and the compensating filter current, clearly illustrating the system's coordinated response. Figure 27 presents the THDi spectrum analysis of the supply current, revealing a distortion level of 1.96%, which is notably lower than the value recorded with the conventional controller in case (B), indicating a significant improvement in harmonic mitigation.

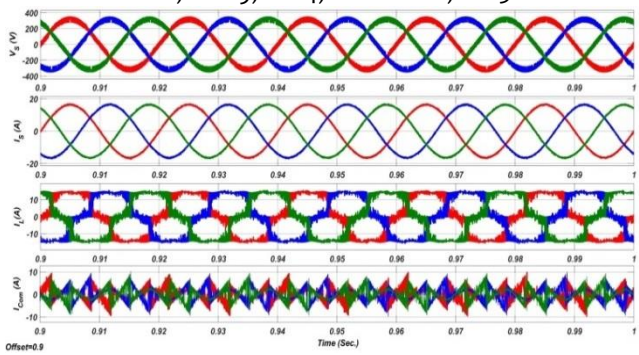

Fig. 26. Three-phase waveforms of source voltage and current with SAPF controlled with optimized adaptive controller using DO algorithm and tested under distorted source voltage conditions for case (C).

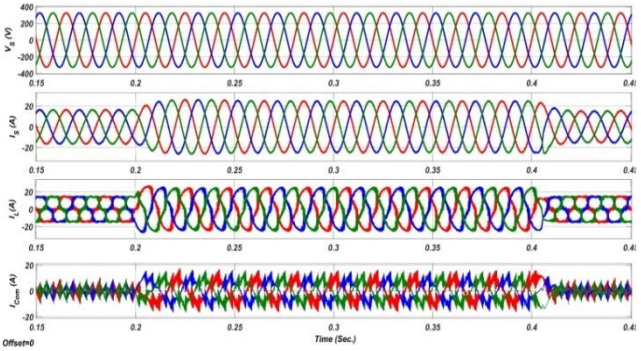

Fig. 28. Three-phase simulation waveforms for Source Voltage, and Current with SAPF controlled with optimized adaptive controller using DO algorithm and tested under load variation conditions for case (C).

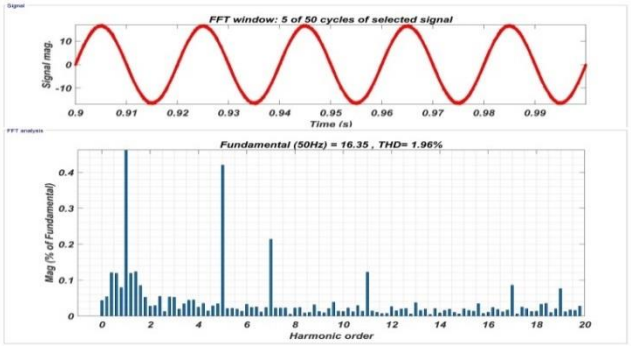

Fig. 27. Source Current waveform, and its FFT harmonic with SAPF controlled with optimized adaptive controller using DO algorithm and tested under distorted source conditions for case (C).

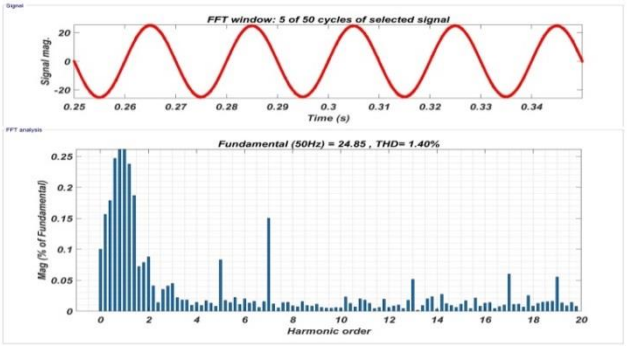

Fig. 29. Source Current waveform, and its FFT harmonic with SAPF controlled with optimized adaptive controller using DO algorithm and tested under load variation conditions for case (C).

7.3.1.4. Simulation with an optimized adaptive controller using the DO algorithm tested under load variation conditions

This section assesses the optimized controller's dynamic performance under severe loading conditions, where the system is subjected to a 150% overload through simultaneous connection of RLC and NLLs. As illustrated in Figure 28, the abrupt application (0.2 sec) and removal (0.4 sec) of the RLC load demonstrates the controller's exceptional regulation capability - maintaining perfect sinusoidal source current throughout the transient. The corresponding FFT analysis in Figure 29 reveals outstanding harmonic suppression, with THDi remaining at an impressively low 1.4% even during peak overload conditions.

As shown in Figure 30, the SAPF controller exhibits exceptional voltage regulation through its dynamic response to load variations. It tracks the DC-link reference with minimal overshoot, error, and settling time, confirming its superior performance. İt observed that the optimized SAPF adaptive controller using the DO algorithm gives an acceptable value for the desired objective functions when tested under different conditions, including ideal and distorted source voltage conditions, and also under dynamic load variation conditions. Thus confirming the efficiency of the chosen DO optimizer.

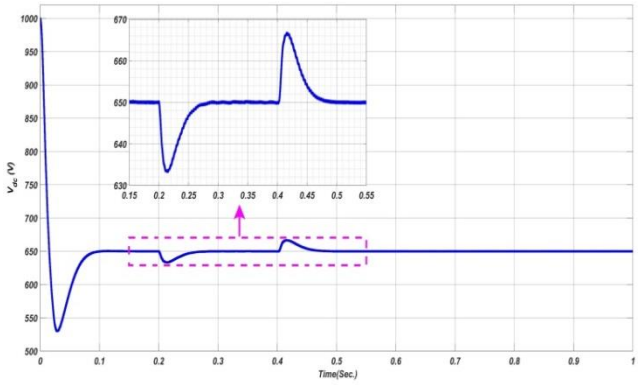

Fig. 30. Response of DC-link voltage of SAPF controlled with an optimized adaptive controller using DO algorithm tested under load variation conditions for case (C).

7.4. Comparison between the conventional and adaptive controllers optimized using the DO algorithm

This section compares the conventional and adaptive controllers under identical conditions, with Table 7 presenting the THDi values for each case. The results reveal similar THD levels for both controllers when dealing with an ideal source and load variations. However, the adaptive controller stands out in scenarios involving a distorted source, thanks to its advanced synchronization algorithm that integrates PSVD and PLL circuits.

Table 7. Comparison between the conventional and adaptive controllers

Comparison cases	THD using a Conventional controller	THD using an Adaptive controller
Ideal source	1.95 %	1.958 %
Distorted source	2.99 %	1.96 %
Load variation	1.43 %	1.4 %

7.5. Comparative Performance Evaluation of Optimization Algorithms under Different Control Strategies

Table 8 presents a detailed performance comparison of four optimization algorithms: DO, AO, MOA, and WSO used for tuning PI controllers in SAPF applications under two operating scenarios (Cases B and C). The comparison includes Total Harmonic Distortion, percentage overshoot, and settling time of the DC-link voltage.

The results indicate that the Dandelion Optimizer (DO) outperforms the other algorithms in both cases, achieving the lowest THD and shortest settling time, thereby confirming its superior dynamic response and robustness. The AO and MOA algorithms show moderate performance, while WSO demonstrates the highest overshoot and settling time, making it the least efficient in terms of response dynamics. These findings are consistent with the convergence behavior shown in Figures 14 and 23, where DO reaches optimal fitness values faster and more consistently than others.

Table 8. Comparative performance summary of optimization algorithms for cases B and C

Algorithm	Case B			Case C		
	THD (%)	Overshoot (%)	Settling Time (s)	THD (%)	Overshoot (%)	Settling Time (s)
DO	1.95	5.4	0.28	1.958	5.1	0.25
AO	1.96	7.2	0.34	1.976	6.9	0.31
MOA	1.952	6.5	0.32	1.963	6.3	0.30
WSO	1.955	8.1	0.36	1.9622	7.7	0.34

8. Conclusion

This research investigates a SAPF solution for PQ enhancement, specifically targeting current harmonic compensation and critical PQ issue mitigation. Two control strategies are employed: a conventional controller and an adaptive controller. Both controllers are optimized using different optimization techniques, having an input variable represented as a PI- PI-Controller's gains and objective functions represent an output, including optimal THDi and Error-values. The performance of these controllers is rigorously evaluated under various operating conditions, including ideal and distorted source voltages, as well as dynamic nonlinear load variations. Results demonstrate that the DO stands out as a robust and efficient metaheuristic algorithm, outperforming other optimization methods in achieving the desired objectives.

Notably, the adaptive controller delivers superior accuracy and performance compared to conventional approaches. By optimizing critical parameters, the SAPF effectively minimizes THDi OF source current, reduces settling time, stabilizes DC-link voltage steady-state error, and mitigates peak overshoot, validating its enhanced efficacy in real-world PQ improvement.

From the previous study, the following conclusions have been reached:

- The proposed SAPF controller techniques effectively compensate for 23.44% of THDi caused by current harmonics from NLLs, reducing the supply current's total harmonic distortion to well within the standard acceptable limit of 5%, and transforming the source current into a clean, sinusoidal waveform.
- By applying optimized tuning methods to the PI controllers, all THDi values are reduced compared to those without tuning, while the DC-link capacitor voltage consistently returns to its reference level without deviation, unlike the behavior observed in unoptimized controllers.
- The DO optimizer delivers exceptional performance, achieving superior accuracy and the strongest correlation with DC-link reference voltage when compared to AO, MOA, and WSO algorithms. It consistently produces the lowest THDi and minimal error values across all scenarios, including impure source voltage conditions and dynamic load variations, outperforming other optimization techniques.
- It is observed that the optimized SAPF adaptive controller using the DO algorithm achieves acceptable values for the desired objective functions in all comparison cases. This confirms the efficiency of the chosen DO optimizer over other techniques, as well as the superiority of the adaptive controller compared to conventional controllers.

This work contributes directly to the advancement of Green and Smart Grid (GAS) technologies, where maintaining high PQ is essential for integrating renewable energy sources, distributed generation, and electric vehicle charging systems. By combining adaptive control techniques with intelligent optimization algorithms, this study contributes to the development of self-regulating, resilient, and energy-efficient smart grids. These grids can effectively adapt to disturbances and load variations while minimizing losses and enhancing overall system stability. Building upon the promising results of this research, several future directions are proposed:

- Extension to multi-objective optimization frameworks that simultaneously consider other power quality indices, such as voltage unbalance, reactive power compensation, and system losses.
- Hybridization of the DO with other metaheuristic or AI-based algorithms to enhance convergence speed, accuracy, and robustness in complex, high-dimensional optimization problems.
- Integration with IoT-enabled and AI-assisted smart grid management systems to allow predictive, self-learning, and adaptive power quality control in future decentralized power networks.

- Application in microgrids and renewable energy-based distribution systems, where PQ challenges are increasingly critical due to the intermittent and fluctuating nature of distributed generation.

- Collectively, the strong emphasis on PI-controller parameter optimization for DC-link voltage and PLL synchronization highlights the practical feasibility of deploying PI-based controllers optimized by metaheuristic algorithms such as the Dandelion Optimizer (DO). This approach confirms that Shunt Active Power Filters (SAPFs) can be effectively controlled and optimized for real-time deployment on high-speed DSP/FPGA platforms, ensuring both rapid dynamic response and operational stability under challenging nonlinear and distorted load conditions. These promising outcomes strongly motivate us to work on this in the future, supporting the practical deployment of power quality solutions in smart grid environments.

Author Contributions

Methodology, A.M.A.S. and A.A.E; Validation, M.H.A., A.A.E, and S.E; Formal analysis, A.M.A.S.; Investigation, A.M.A.S. and A.A.E.; Resources, A.M.A.S., A.A.E., M.H.A and S.E.; Software, M.H.A. and A.A.E; Data curation, M.H.A and S.E..; Writing—original draft, A.M.A.S.; Writing review & editing, A.M.A.S., M.H.A., A.A.E and S.E.; Supervision, A.M.A.S.. All authors have read and agreed to the published version of the manuscript.

References

[1] L. Morán, J. Dixon, and M. Torres, "Active Power Filters," in Power Electronics Handbook, Fourth Edition, Elsevier, pp. 1341–1379, 2017. doi: 10.1016/B978-0-12-811407-0.00046-5.

[2] A. M. Sulehri, N. Jeelani, and A. A. Ikram, "Power quality improvement in an AC network using artificial neural network and hysteresis band current controller," Ingenieria e Investigacion, vol. 38, no. 3, pp. 42–49, 2018, doi: 10.15446/ING.INVESTIG.V38N3.67885.

[3] N. D. Tuyen, G. Fujita, and M. N. bin Muhtazaruddin, "Notch adaptive filter solution under unbalanced and/or distorted PCC voltage for 3-phase 3-wire shunt active power filter," Electrical Engineering, vol. 98, no. 3, pp. 321–332, Sep. 2016, doi: 10.1007/s00202-016-0362-9.

[4] X. Li and B. Li, "A Decoupling Control Method for Shunt Hybrid Active Power Filter Based on Generalized Inverse System," Journal of Electrical and Computer Engineering, vol. 2017, 2017, doi: 10.1155/2017/5232507.

[5] O. Prakash Mahela and A. Gafoor Shaik, "Topological aspects of power quality improvement techniques: A comprehensive overview," Renewable and Sustainable Energy Reviews, vol. 58. Elsevier Ltd, pp. 1129–1142, May 01, 2016. doi: 10.1016/j.rser.2015.12.251.

[6] S. Tiyarachakun, K. Areerak, and K. Areerak, "Instantaneous power theory with fourier and optimal predictive controller design for shunt active power filter," Modelling and Simulation in Engineering, vol. 2014, 2014, doi: 10.1155/2014/381760.

[7] Y. Hoon, M. A. M. Radzi, M. A. A. M. Zainuri, and M. A. M. Zawawi, "Shunt active power filter: A review on phase synchronization control techniques," Electronics (Switzerland), vol. 8, no. 7. MDPI AG, Jul. 01, 2019. doi: 10.3390/electronics8070791.

[8] C. I. Garcia, F. Grasso, A. Luchetta, M. C. Piccirilli, L. Paolucci, and G. Talluri, "A comparison of power quality disturbance detection and classification methods using CNN, LSTM and CNN-LSTM," Applied Sciences (Switzerland), vol. 10, no. 19, pp. 1–22, Oct. 2020, doi: 10.3390/app10196755.

[9] Y. Hoon, M. A. A. M. Zainuri, A. S. Al-Ogaili, A. N. Al-Masri, and J. Teh, "Active Power Filtering under Unbalanced and Distorted Grid Conditions Using Modular Fundamental Element Detection Technique," IEEE Access, vol. 9, pp. 107502–107518, 2021, doi: 10.1109/ACCESS.2021.3101238.

[10] Y. Fang and J. Fei, "Adaptive Backstepping Current Control of Active Power Filter Using Neural Compensator," Mathematical Problems in Engineering, vol. 2019, 2019, doi: 10.1155/2019/5130738.

[11] A. Lakum and V. Mahajan, "A novel approach for optimal placement and sizing of active power filters in radial distribution system with nonlinear distributed generation using adaptive grey wolf optimizer," Engineering Science and Technology, an International Journal, vol. 24, no. 4, pp. 911–924, Aug. 2021, doi: 10.1016/j.jestch.2021.01.011.

[12] T. A. H. Alghamdi, F. Anayi, and M. Packianather, "Optimal Design of Passive Power Filters Using the MRFO Algorithm and a Practical Harmonic Analysis Approach including Uncertainties in Distribution Networks," Energies, vol. 15, no. 7, Apr. 2022, doi: 10.3390/en15072566.

[13] D. Buła, D. Grabowski, and M. Maciążek, "A Review on Optimization of Active Power Filter Placement and Sizing Methods," Energies, vol. 15, no. 3. MDPI, Feb. 01, 2022. doi: 10.3390/en15031175.

[14] M. Kumar, M. A. Uqaili, Z. A. Memon, and B. Das, "Experimental Harmonics Analysis of UPS (Uninterrupted Power Supply) System and Mitigation Using Single-Phase Half-Bridge HAPF (Hybrid Active Power Filter) Based on Novel Fuzzy Logic Current Controller (FLCC) for Reference Current Extraction (RCE)," Advances in Fuzzy Systems, vol. 2022, 2022, doi: 10.1155/2022/5466268.

[15] F. Alasali, K. Nusair, H. Foudeh, W. Holderbaum, A. Vinayagam, and A. Aziz, "Modern Optimal Controllers for Hybrid Active Power Filter to Minimize Harmonic Distortion," Electronics (Switzerland), vol. 11, no. 9, May 2022, doi: 10.3390/electronics11091453.

[16] L. F. J. Meloni, F. L. Tofoli, A. J. J. Rezek, and E. R. Ribeiro, "Modeling and Experimental Validation of a Single-Phase Series Active Power Filter for Harmonic

Voltage Reduction," IEEE Access, vol. 7, pp. 151971–151984, 2019, doi: 10.1109/ACCESS.2019.2947917.

[17] Y. Fang, J. Fei, and T. Wang, "Adaptive Backstepping Fuzzy Neural Controller Based on Fuzzy Sliding Mode of Active Power Filter," IEEE Access, vol. 8, pp. 96027–96035, 2020, doi: 10.1109/ACCESS.2020.2995755.

[18] M. Kadem, A. Semmah, P. Wira, and S. Dahmani, "Fuzzy logic-based instantaneous power ripple minimization for direct power control applied in a shunt active power filter," Electrical Engineering, vol. 102, no. 3, pp. 1327–1338, Sep. 2020, doi: 10.1007/s00202-020-00943-6.

[19] A. Bielecka and D. Wojciechowski, "Stability Analysis of Shunt Active Power Filter with Predictive Closed-Loop Control of Supply Current," Energies, Volume 14, Issue 8, 2208,2021, doi: 10.3390/en14.

[20] S. F. Al-Gahtani and R. M. Nelms, "A frequency adaptive control scheme for a three-phase shunt active power filter," Electrical Engineering, vol. 103, no. 1, pp. 595–606, Feb. 2021, doi: 10.1007/s00202-020-01105-4.

[21] M. Pichan, M. Seyyedhosseini, and H. Hafezi, "A New DeadBeat-Based Direct Power Control of Shunt Active Power Filter with Digital Implementation Delay Compensation," IEEE Access, vol. 10, pp. 72866–72878, 2022, doi: 10.1109/ACCESS.2022.3188685.

[22] M. Sivasubramanian, C. S. Boopathi, S. Vidyasagar, V. Kalyanasundaram, and S. Kaliyaperumal, "Performance Evaluation of Seven Level Reduced Switch ANPC Inverter in Shunt Active Power Filter with RBFNN-Based Harmonic Current Generation," IEEE Access, vol. 10, pp. 21497–21508, 2022, doi: 10.1109/ACCESS.2021.3064715.

[23] S. Sharma, V. Verma, M. Tariq, and S. Urooj, "Reduced Sensor-Based Harmonic Resonance Detection and its Compensation in Power Distribution System With SAPF," IEEE Access, vol. 10, pp. 59942–59958, 2022, doi: 10.1109/ACCESS.2022.3176366.

[24] J. Yu, Y. Xu, Y. Li, and Q. Liu, "An Inductive Hybrid UPQC for Power Quality Management in Premium-Power-Supply-Required Applications," IEEE Access, vol. 8, pp. 113342–113354, 2020, doi: 10.1109/ACCESS.2020.2999355.

[25] J. Han, X. Li, Y. Jiang, and S. Gong, "Three-Phase UPQC Topology Based on Quadruple-Active-Bridge," IEEE Access, vol. 9, pp. 4049–4058, 2021, doi: 10.1109/ACCESS.2020.3047961.

[26] A. Baliyan, M. Jamil, M. Rizwan, I. Alsaidan, and M. Alaraj, "An Intelligent PI Controller-Based Hybrid Series Active Power Filter for Power Quality Improvement," Mathematical Problems in Engineering, vol. 2021, 2021, doi: 10.1155/2021/6565841.

[27] A. Khan et al., "Hardware-in-the-Loop Implementation and Performance Evaluation of Three-Phase Hybrid Shunt Active Power Filter for Power Quality Improvement," Mathematical Problems in Engineering, vol. 2021, 2021, doi: 10.1155/2021/8032793.

[28] S. K. El-Sayed and A. M. A. soliman, "Power quality improvement for distribution network by design of two control strategies for active power filter," International Journal of Engineering and Advanced Technology Studies, Vol.3, No.3, pp.1-22, October 2015. [Online]. Available: www.eajournals.org.

[29] T. M. T. Thentral et al., "Development of Control Techniques Using Modified Fuzzy Based SAPF for Power Quality Enhancement," IEEE Access, vol. 9, pp. 68396–68413, 2021, doi: 10.1109/ACCESS.2021.3077450.

[30] A. A. Eid, A. M. A. Soliman, and M. A. Mehanna, "Optimize Gain Values of PI-Controller for Active Power Filter Using Mayfly Algorithm," International Journal Of Renewable Energy Research, Vol.12, No.4, December 2022, doi:10.20508/ijrer.v12i4.13413.g8597.

[31] A. A. Eid, A. M. A. Soliman, and M. A. Mehanna, "Dynamic performance optimization of shunt active power filter to eliminate total harmonic distortion", Journal of Al-Azhar University Engineering Sector, Vol. 18, No. 66, 116–128, January 2023,doi:10.21608/auej.2023.283033.

[32] A. M. A. Soliman, S. K. El-Sayed, and M. A. Mehanna, "Effect of Utility Voltage Distortion on the Performance of Different Control Strategies for Shunt Active Power Filter," European Journal of Engineering Research and Science, vol. 2, no. 8, p. 27, Aug. 2017, doi: 10.24018/ejers.2017.2.8.445.

[33] Z. Ali, N. Christofides, K. Saleem, A. Polycarpou, and K. Mehran, "Performance evaluation and benchmarking of PLL algorithms for grid-connected RES applications," IET Renewable Power Generation, vol. 14, no. 1, pp. 52–62, Jan. 2020, doi: 10.1049/iet-rpg.2019.0434.

[34] J. K. Sao, R. T. Naayagi, G. Panda, R. D. Patidar, and S. D. Swain, "SAPF Parameter Optimization with the Application of Taguchi SNR Method," Electronics (Switzerland), vol. 11, no. 3, Feb. 2022, doi: 10.3390/electronics11030348.

[35] D. Prasad Acharya, S. Choudhury, and N. Nayak, "Optimal Design of Shunt Active Power Filter for Power Quality Improvement and Reactive Power Management Using nm-Predator Prey Based Firefly Algorithm," International Journal Of Renewable Energy Research, Vol.12, No.1, March. 2022, doi:10.20508/ijrer.v12i1.12705.g8412.

[36] H. Acikgoz, O. F. Kececioglu, A. Gani, M. Tekin, and M. Sekkeli, "Robust control of shunt active power filter using interval type-2 fuzzy logic controller for power quality improvement," Tehnicki Vjesnik, vol. 24, pp. 363–368, Sep. 2017, doi: 10.17559/TV-20161213004749.

[37] K. Rameshkumar and V. Indragandhi, "Real Time Implementation and Analysis of Enhanced Artificial

Bee Colony Algorithm Optimized PI Control algorithm for Single Phase Shunt Active Power Filter," Journal of Electrical Engineering and Technology, vol. 15, no. 4, pp. 1541–1554, Jul. 2020, doi: 10.1007/s42835-020-00437-2.

[38] B. Mahesh Babu, N. Uday Kumar, K. Santhosh Kumar, A. Amarendra,and B. Bindhu, " SAPF for Power Quality Improvement Based on PSODE Optimization Algorithm," International Journal of Engineering and Advanced Technology, vol. 9, no. 3, pp.3454–3460, February 2020,doi:10.35940/ijeat.B2517.029320.

[39] M. Iqbal et al., "Neural Networks Based Shunt Hybrid Active Power Filter for Harmonic Elimination," IEEE Access, vol. 9, pp. 69913–69925, 2021, doi: 10.1109/ACCESS.2021.3077065.

[40] S. Kakkar et al., "Design and Control of Grid-Connected PWM Rectifiers by Optimizing Fractional Order PI Controller Using Water Cycle Algorithm," IEEE Access, vol. 9, pp. 125941–125954, 2021, doi: 10.1109/ACCESS.2021.3110431.

[41] R. Kumar, H. O. Bansal, A. R. Gautam, O. P. Mahela, and B. Khan, "Experimental Investigations on Particle Swarm Optimization Based Control Algorithm for Shunt Active Power Filter to Enhance Electric Power Quality," IEEE Access, vol. 10, pp. 54878–54890, 2022, doi: 10.1109/ACCESS.2022.3176732.

[42] V. A. G. Kumar and D. M. Reddy, "Optimized PI tuning of DG-Integrated Shunt Active Power Filter Using Biogeography-Based Optimization Algorithm," Journal Europeen des Systemes Automatises, vol. 56, no. 6, pp. 907–916, Dec. 2023, doi: 10.18280/jesa.560602.

[43] B. M. Babu et al., "Power Quality Improvement based on VSHDE Algorithm Incorporating Shunt Active Power Filter,"J. Electrical Systems , Vol. 19 No. 1,2023,doi:10.52783/jes.15.

[44] S. Ali, A. Bhargava, A. Saxena, A. S. Almazyad, K. M. Sallam, and A. W. Mohamed, "An Amended Crow Search Algorithm for Hybrid Active Power Filter Design," Processes, vol. 11, no. 9, Sep. 2023, doi: 10.3390/pr11092550.

[45] F. Bourourou, S. Ahmed Tadjer, and I. Habi, "Three-Dimensional Fuzzy Logic Applied to DC Voltage Regulation in Active Power Filter of PV System," International Journal of Smart Grid, Vol.7, No.2,June.2023,doi:10.20508/ijsmartgrid.v7i2.287.g274.

[46] G. V. A. Kumar and M. D. Reddy, "Mitigation of Grid Current Harmonics by ABC-ANN based Shunt Active Power Filter," Journal of Advanced Research in Applied Sciences and Engineering Technology, vol. 33, no. 1, pp. 285–298, Dec. 2023, doi: 10.37934/araset.33.1.285298.

[47] S. K. Yadav, A. Patel, and H. D. Mathur, "PSO-Based Online PI Tuning of UPQC-DG in Real-Time," IEEE Open Journal of Power Electronics, vol. 5, pp. 1419–1431, 2024, doi: 10.1109/OJPEL.2024.3445719.

[48] R. Mallajoshula and I. E. S. Naidu, "Power quality improvement using PV fed series active power filter with enhanced Jaya optimized PI controller," International Journal of Power Electronics and Drive Systems, vol. 15, no. 4, pp. 2199–2213, Dec. 2024, doi: 10.11591/ijpeds.v15.i4.pp2199-2213.

[49] D. Bakria et al., "An optimized shunt active power filter using the golden Jackal optimizer for power quality improvement," Scientific Reports, vol. 15, no. 1, Dec. 2025, doi: 10.1038/s41598-025-00204-1.

[50] N. Rajesh Kumar Gowd and B. Srikanth Goud, "Power Quality Enhancement in PV Fed UPQC using Adaptive Lizard Algorithm," INTERNATIONAL JOURNAL of SMART GRID, Vol.9, No.1, March.2025,doi:10.20508/ijsmartgrid.v9i1.407.g378.

[51] P. Riyas and S. A. Lakshmanan, "Optimal tuning of PI based LF for three-phase SRF PLL synchronization system using pity beetle algorithm under grid abnormalities," Scientific Reports, vol. 15, no. 1, Dec. 2025, doi: 10.1038/s41598-025-03530-6.

[52] A. K. Mishra, P. K. Ray, R. K. Mallick, A. Mohanty, and S. R. Das, "Adaptive fuzzy controlled hybrid shunt active power filter for power quality enhancement," Neural Computing and Applications, vol. 33, no. 5, pp. 1435–1452, Mar. 2021, doi: 10.1007/s00521-020-05027-x.

[53] M. A. Mansor, K. Hasan, M. M. Othman, S. Z. B. M. Noor, and I. Musirin, "Construction and Performance Investigation of Three-Phase Solar PV and Battery Energy Storage System Integrated UPQC," IEEE Access, vol. 8, pp. 103511–103538, 2020, doi: 10.1109/ACCESS.2020.2997056.

[54] D. Azhagesan, M. Periyasamy, S. Manickavasagam Parvathy, M. Sridharan, and C. B. Baladhandautham, "Predictive current control of FL-shunt active power filter for dynamic and heterogeneous load compensation," Electrical Engineering, vol. 103, no. 4, pp. 2147–2160, Aug. 2021, doi: 10.1007/s00202-021-01224-6.

[55] IEEE Standard 519-1981. Recommended practice and requirement for harmonic control in electric power systems, The Institute of Electrical and Electronics Engineers,1993,doi:10.1109/IEEESTD.1993.114370.

[56] IEEE Standard 519-1992. Recommended practice and requirement for harmonic control in electric power systems, The Institute of Electrical and Electronics Engineers,2014,doi:10.1109/IEEESTD.2014.6826459.

[57] IEEE Standard 519-2022. Recommended practice and requirement for harmonic control in electric power systems, , The Institute of Electrical and Electronics Engineers,2022,doi:10.1109/IEEESTD.2022.9848440.

[58] B. M. Babu, "Improvement of power quality using shunt active power filter based on gravitational search algorithm," i-manager's Journal on Instrumentation and Control Engineering, vol. 7, no. 4, p. 26, 2019, doi:

[59] M. H. Ali, M. H. Ali, A. M. A. Soliman, M. F. Ahmed, and A. H. Adel , "Optimization of Reactive Power Dispatch Considering DG Units Uncertainty by Dandelion Optimizer", International Journal Of Renewable Energy Research, Vol.12, No.4, December 2022,doi:10.20508/ijrer.v12i4.13573.g8606.

[60] S. Zhao, T. Zhang, S. Ma, and M. Chen, "Dandelion Optimizer: A nature-inspired metaheuristic algorithm for engineering applications,"Engineering Applications of Artificial Intelligence, vol.114, 105075, September. 2022 ,doi:10.1016/j.engappai.2022.105075.